Electronic supplementary information (ESI) for

$Ag_{18}(\mu_8\text{-}S)(p\text{-}TBBT)_{16}(PPh_3)_8$: Symmetry Breaking Induced by Core to Generate Chirality

*Fan Tian, and Rong Chen**

School of Chemistry and Environmental Engineering, Wuhan Institute of Technology, Xiongchu Avenue, Wuhan, 430073, PR China

** Corresponding author: Prof. R. Chen, E-mail: rchenhku@hotmail.com*

Tel.: (+86)13659815698; Fax: (+86)2787195680.

Table of Content

Materials

Silver nitrate ($AgNO_3$, AR), sodium borohydride (98%), methanol (MeOH, AR) and dichloromethane (CH_2Cl_2, AR) were purchased from Sinopharm (Shanghai, China). 4-tert-Butylbenzylthiol (p-TBBT, 97%), triphenylphosphine (PPh_3, 99%) and tetrakis(triphenylphosphine) palladium ($Pd(PPh_3)_4$, 99%) were purchased from Meryer (Shanghai, China). The water used in all experiments was ultrapure. All the reagents were used directly without further purification.

Methods

Synthesis and crystallization of $Ag_{18}S(p\text{-}TBBT)_{16}(PPh_3)_8$ nanocluster: *120 mg $AgNO_3$, 25 mg of $Pd(PPh_3)_4$ and 500 mg PPh_3 were dispersed in 10 mL of methanol, followed by addition of 40 mL of dichloromethane, forming an orange solution. Then, 150 μL of p-TBBT was added. The solution was stirred for more than 1 hour to assure that all the metal atoms were fully coordinated. After that, 1 mL of an $NaBH_4$ aqueous solution (60 mg/mL) was added in. The solution then quickly turned to grey, indicating the formation of nanoparticles. A reddish-grey solution was obtained after maintained the reaction under 10±2°C for 24 hours. $Ag_{18}S$ single crystals suitable for X-ray diffraction study were grown by slowly layering MeOH in to the solution at 4 °C for one week. The yield of the cluster is estimated to be ~23% according to the mass of crystals based on the Ag element.*

Synthesis and purification of $Ag_{33}(SR)_{12}(PPh_3)_4$ nanocluster: *The synthesis and crystallization of Ag_{33} nanocluster are identical to the previous report[1].*

Synthesis and purification of $Ag_{23}(SR)_{12}(PPh_3)_4$ nanocluster: *The synthesis and crystallization of Ag_{23} nanocluster are referring to the recent report[2]..*

Characterization

The UV-vis spectrum and photoluminescence spectrum were recorded by HITACHI UH4510 Spectrophotometer with dichloromethane as solvent. X-ray photoelectron spectroscopy (XPS) was performed on an ESCALAB 250 spectrometer with monochromated Al Kα radiation as the excitation source. X-ray diffraction data was recorded on an XtaLAB AFC12 (RINC): Kappa single diffractometer (Rigaku, Japan) with Cu Kα radiation (λ = 1.54184 Å). The crystal was kept at 100.00(10) K during data collection. NMR spectrum of the $Ag_{18}S$ crystals were recorded at room temperature on a Bruker AV-500 spectrometer with chloroform-d_3 as solvent and TMS (0.0 ppm) as an internal reference. The contribution from chloroform-d_3 (integral 0.54) in the peaks intergration is excluded by also using TMS (integral 1) as an quantative reference.

Computational details

*The electronic structure of $Ag_{18}S$ nanocluster was calculated based on density functional theory (DFT) via CP2K/Quickstep program (version 6.1)[3]. By employing localized Gaussian and plane wave basis sets to describe the electron density[4], the program can handle systems with hundreds of atoms efficiently, which is suitable for nanoclusters' calculations. The wave functions were expanded in an molecular optimized double-ζ Gaussian basis sets (DZVP- MOLOPT-GTH)[5] with an auxiliary plane-wave basis set with a cutoff energy of 320 Ry. Core electrons was modeled by the scalar relativistic norm-conserving Goedecker−Teter− Hutter (GTH) potentials[6-8] with 11, 6, 5, 4 and 1 valence electrons for Ag, S, P, C and H atoms, respectively. All simulations were performed using the generalized gradient-corrected exchange-correlation functional developed by Perdew, Burke, and Ernzerhof (PBE)[9]. The initial atomic coordinates and chemical compositions of the clusters were based on the experimental crystal structures, with corrections for the effect of disorder. In a typical calculation, an $Ag_{18}S$ nanocluster with full of ligands were placed in a 35 Å cubic simulation. The cluster was optimized in the box with periodic boundary conditions switched off by using the wavelet Poisson solver using limited-memory Broyden−Fletcher−Goldfarb−Shanno (BFGS) algorithm until the forces acting on each atoms bellowing 0.005 eV/Å. After the optimization converged, the obtained structure is further optimized with the conjugate gradient algorithm to check whether it is local minimal. Ground state DFT calculation was employed to obtained the projected density of states and total valence density. The obtained results were further analysis by density derived electrostatic and chemical (DDEC) method[10-12]. TDDFPT calculations is also performed in the same framework with 350 excitation states been calculated. The obtained excitations are extracted and broadening with FWHM of 0.1 eV using Multiwfn program (version: 3.6) [13]. The computed spectra systematically underestimate all transition energies by ~0.6 eV, which is understandable based on the properties of the DFT functional used in the calculation. We therefore corrected it in the spectra plot to enable a better visual comparison to experiment. VESTA is used for molecular orbitals visualization[14]. TDDFT was also performed on Gaussian 16 package[15] with a simplified $Ag_{18}S(SCH_3)_{16}(PC_3H_9)_8$ model with the R groups in ligands replaced by $–CH_3$ in b3lyp level to get the electronic circular dichroism (ECD). We employed basis sets of 6–31 G** for H, C, P and S atoms. The LANL2DZ basis set was used for silver atoms.*

The mass spectroscopy analysis

The mass spectra were recorded in both positive ion mode and negative mode on a hybrid quadrupole time-of-flight mass spectrometer (FT-ICR-MS SolariX 7T, Bruker Daltonics, Bremen) with an Electrospray Ionization (ESI-MS) ion source. We have tried ESI-MS for both the crystals and the powder products by varying the gas flow, caplillary voltage and tuber temperature of the sampling, but no the molecular ions signal of the nanocluster is found in the spectrum, either with the addition of Cs^+ or other reagent to make the molecular charged. Figure S1 is one of the obtained spectrum of the powder products in the presence of Cs^+. As shown in the figure, all the detected signals are blew 3500 Da both in positive mode and negative mode.

Those signals exhibit limited isotope distributions, which definitely not contributed from the nanoclusters as the 18 Ag atoms would produce abundant isotope signals. It should be noting that MS cannot be useful if the products or impurities cannot be ionized efficiently. Furthermore, the analysis conditions used in the spectrometer are sometimes harsh for the analyte, which may make the analyte decomposing before being detected by the spectrometer. The absence of the signals of $Ag_{18}S$ nanocluster, therefore, might be either induced by the reason that they are not efficiently ionized or just being decomposed in the characterization.

X-ray single-crystal analysis

Suitable crystals of $Ag_{18}S$ nanocluster was selected respectively and the diffraction data of the crystals was collected on an on a XtaLAB AFC12 (RINC): Kappa single diffractometer (Rigaku, Japan) with Cu Kα radiation (λ = 1.54184 Å). The crystal was kept at 100.00(10) K during data collection. The data was processed and reduction using CrysAlisPro[16]. Using Olex2[17] , the structure was solved with the ShelXS[18] structure solution program using direct methods and refined with the ShelXL [19] refinement package using least squares minimization. There are 18035 independent reflections collected and 858 parameters selected to be refined. 14 restraints (DFIX, DELU, ISOR and RIGU etc.) used in the refinement to make some unreasonable bond lenghs and the Ueq of *some carbon atoms reasonable. A solvent mask was calculated and 2132 electrons were found in a volume of 8336 Å^3 in 2 voids, which corresponding to about 29.625 disorderd methanol molecular in the cell. The final R indexs for all data collected are R_1 = 0.0623 and wR_2 = 0.1599. Detailed crystal data and structure refinements are provided in Supplementary Table S2. The corresponding crystallographic data of those clusters are also deposited in The Cambridge Crystallographic Data Centre (https://www.ccdc.cam.ac.uk) with CCDC numbers of 1940148.*

Supporting Figures

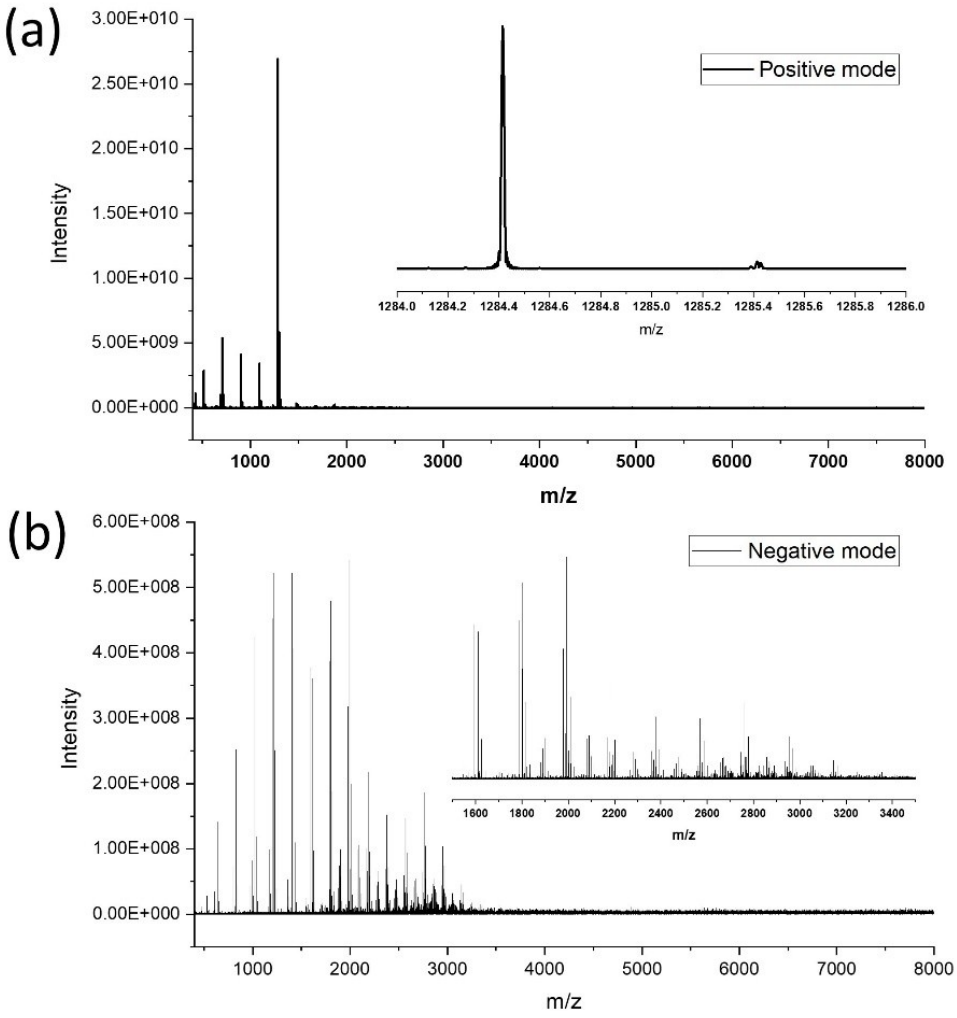

Figure S1. ESI-MS spectra with positive and negative mode of the crystal products in the presence of Cs^{+}.

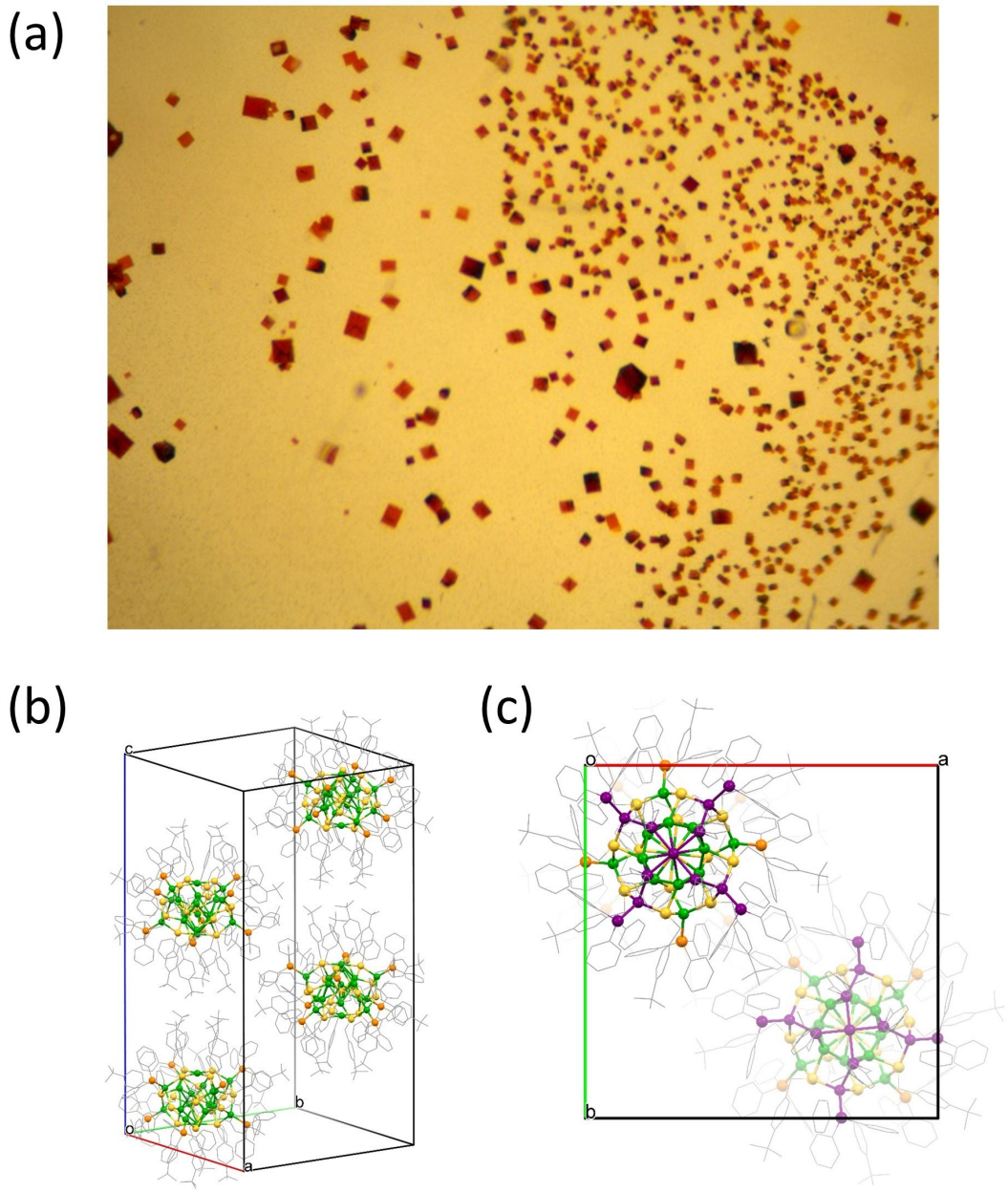

Figure S2 Photograph (a) and visualization of the cell contents (b and c) of $Ag_{18}S$ nanoclusters with packing mode of the obtained single crystal products.

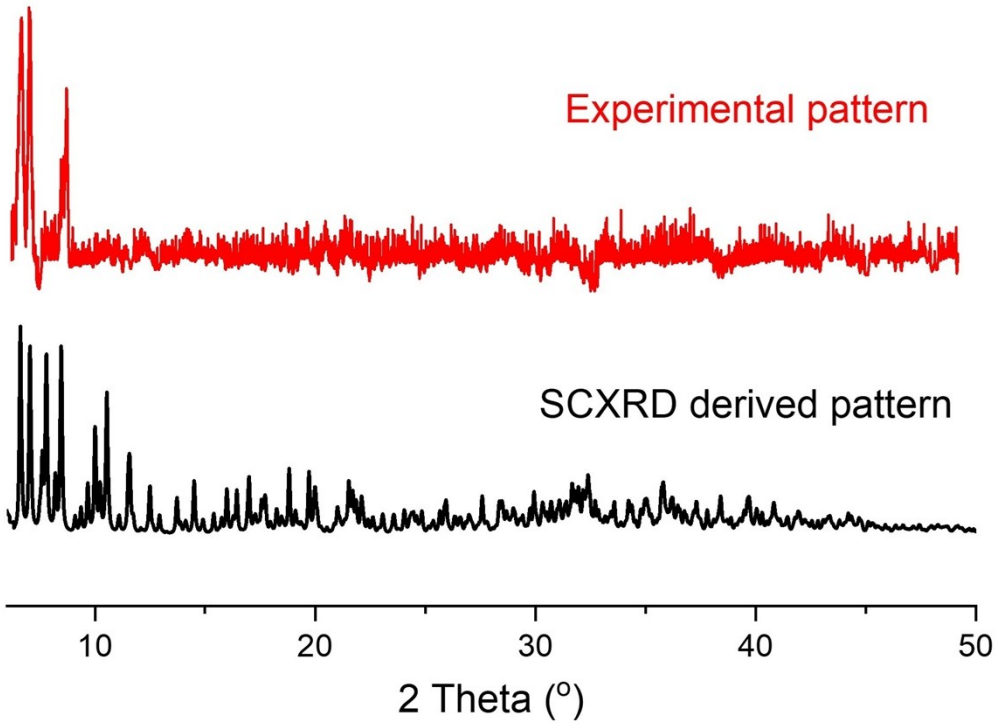

Figure S3 the comparsion of powder XRD pattern and the SCXRD derived pattern of the as prepared crystal products.

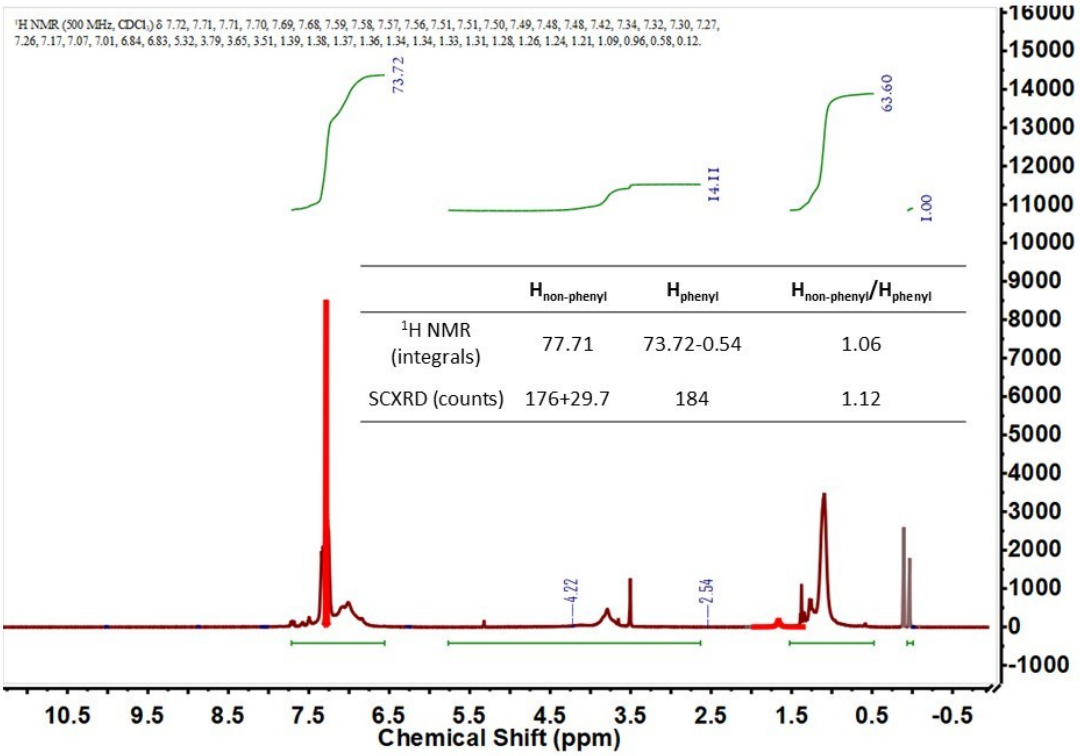

	$H_{non\text{-}phenyl}$	H_{phenyl}	$H_{non\text{-}phenyl}/H_{phenyl}$
^{1}H NMR (integrals)	77.71	73.72-0.54	1.06
SCXRD (counts)	176+29.7	184	1.12

Figure S4 ^{1}H NMR spectrum of the crystal products. Peaks ascribed to the impurity and solvent are colored in red. The integration of peaks for phenyl protons and non-phenyl protons are from 6.5 to 7.8 and 0.5 to 5.8 ppm, respectively. A integral of 0.54 at 7.28 ppm ascrbing to the solvent is excluded in the H_{phenyl} estimation.

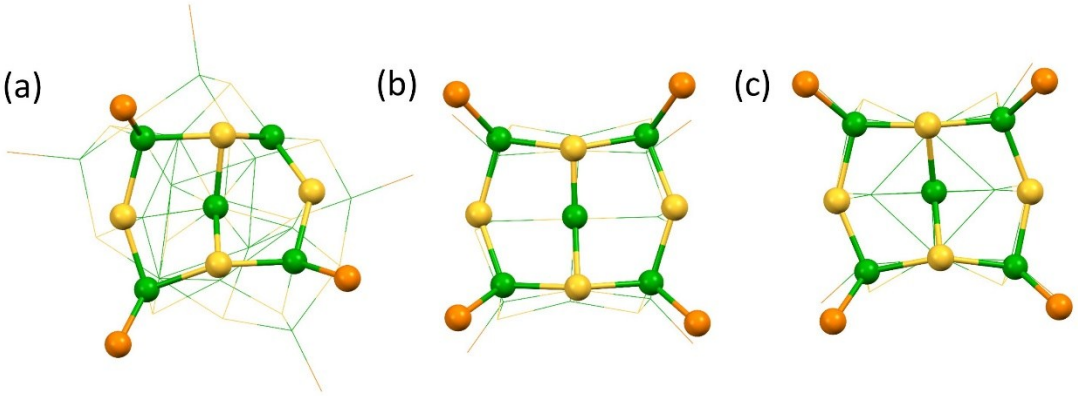

Figure S5 $Ag_5S_4P_3$ unit in $Ag_{18}S(p\text{-}TBBT)_{16}(PPh_3)_8$ nanocluster and $Ag_5S_4P_4$ units in $Ag_{14}S$(b) and Ag_{14} (c) nanoclusters.

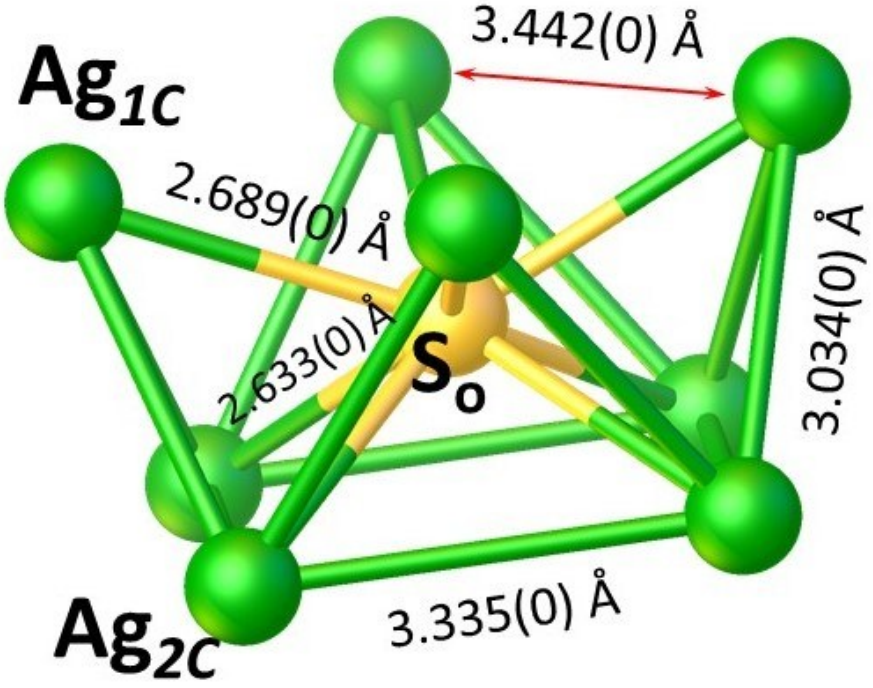

Figure S6 Crown-like geometry of the core SAg_8 motif of $Ag_{18}S$ nanocluster.

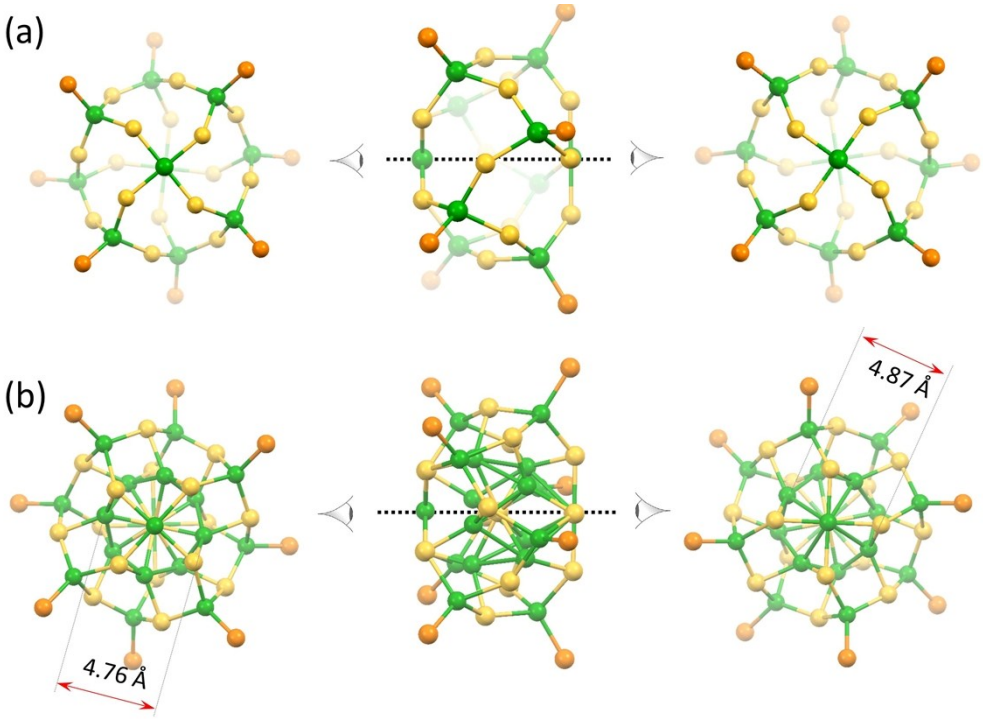

Figure S7 Skeleton illustrations of the $Ag_{10}S_{16}P_8$ shell (a) and the $Ag_{18}S$ kernel (b) structures viewed along the C_4 rotation axis from different side.

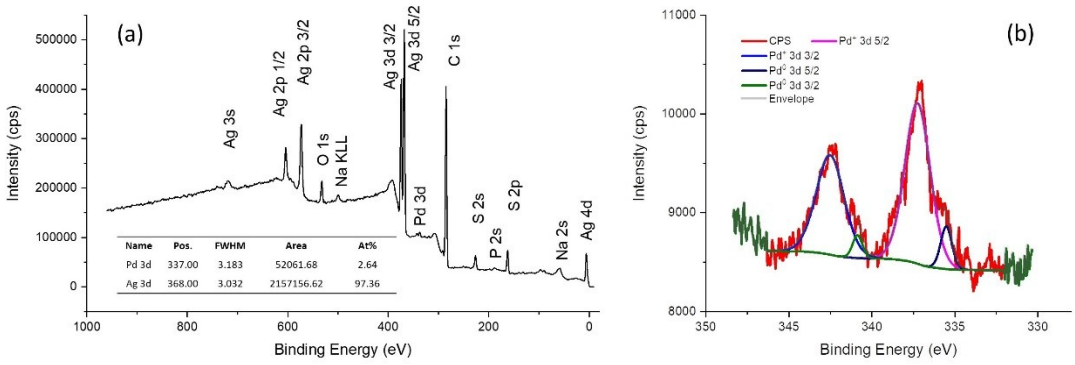

Figure S8 Survey XPS spectrum (a) and high-resolution Pd 3d spectrum of the obtained $Ag_{18}S$ crystals.

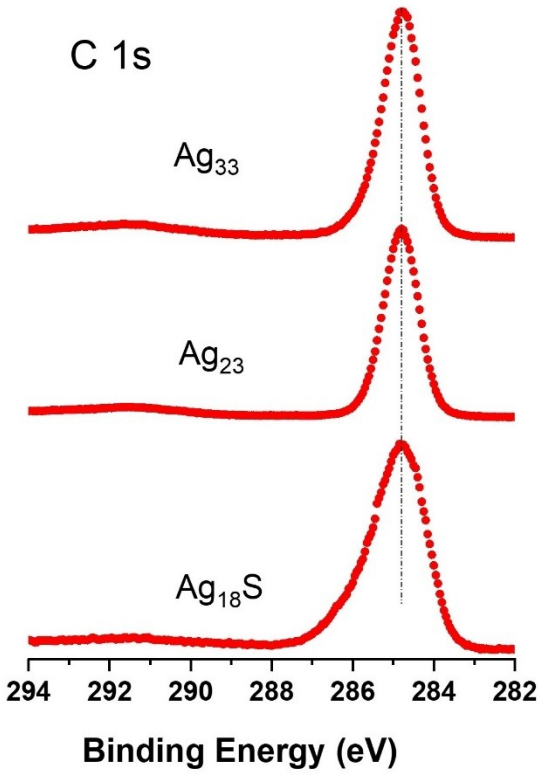

Figure S9 C 1s high resolution XPS of Ag_{33} (top), Ag_{23} (middle) and $Ag_{18}S$ (bottom) nanoclusters.

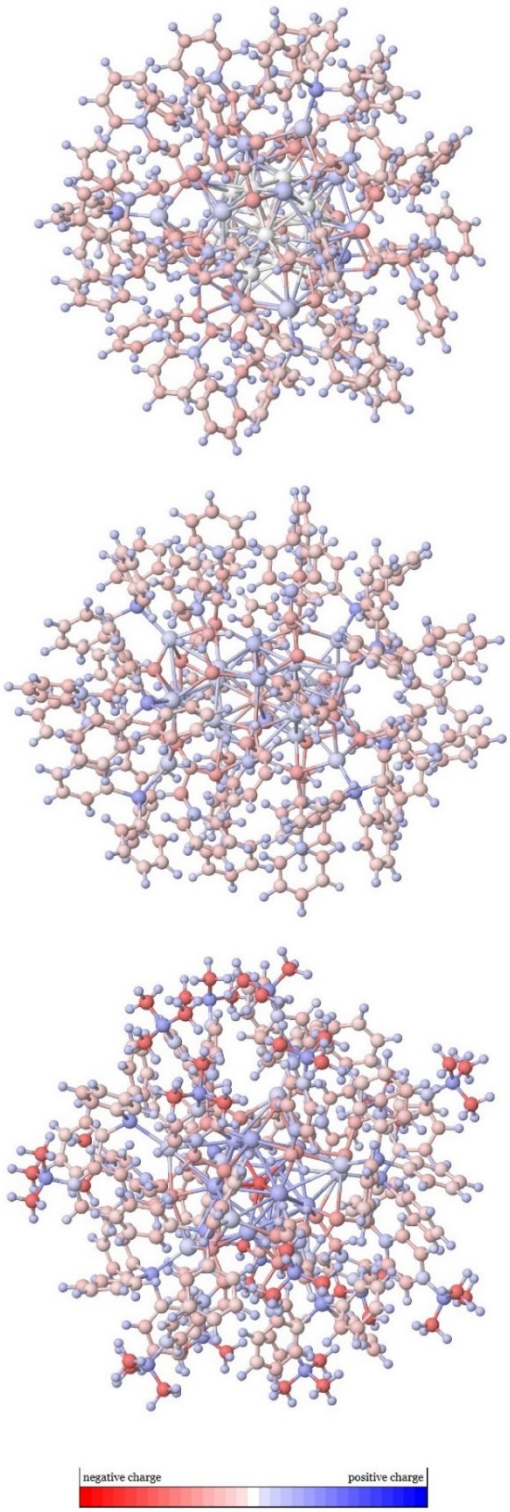

Figure S10 Net atomic charge visualizations of Ag_{33} (the top), Ag_{23} (the middle) and $Ag_{18}S$ the (bottom) nanoclusters derived from the density derived electrostatic and chemical (DDEC) method[10-12].

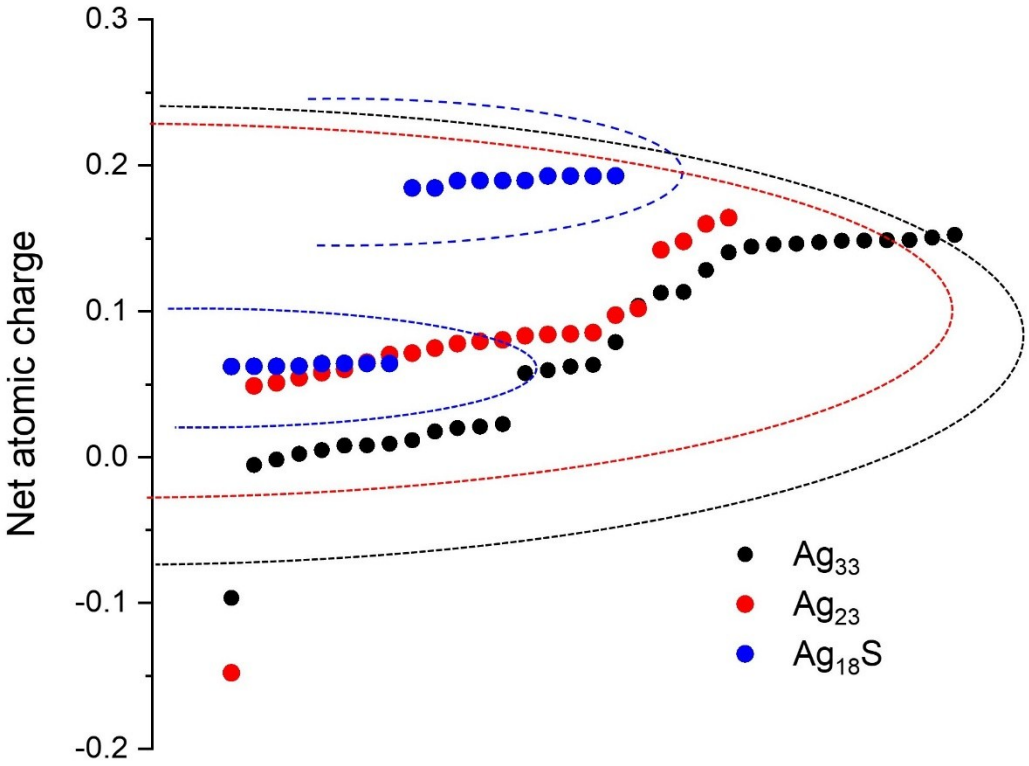

Figure S11 Net atomic charge distributions of Ag atoms in Ag_{33}, Ag_{23} and $Ag_{18}S$ nanoclusters. Each dot represents an Ag atom.

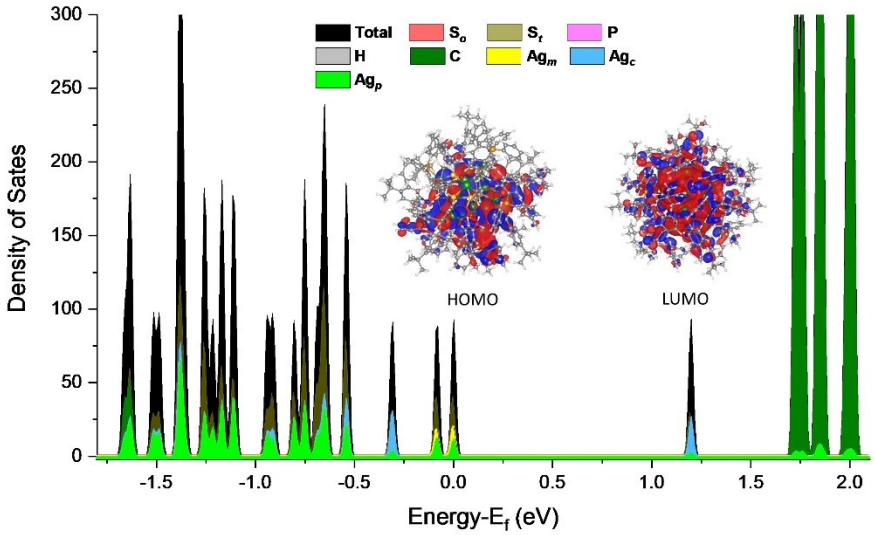

Figure S12 Partial density of states projected for different kinds of atoms of $Ag_{18}S$ nanocluster.

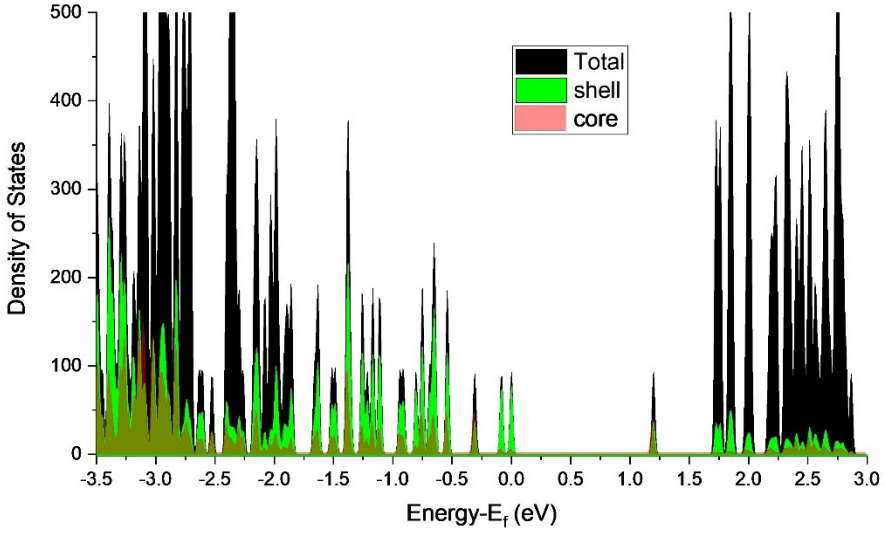

Figure S13 Partial density of states projected for core and shell of $Ag_{18}S$ nanoclusters.

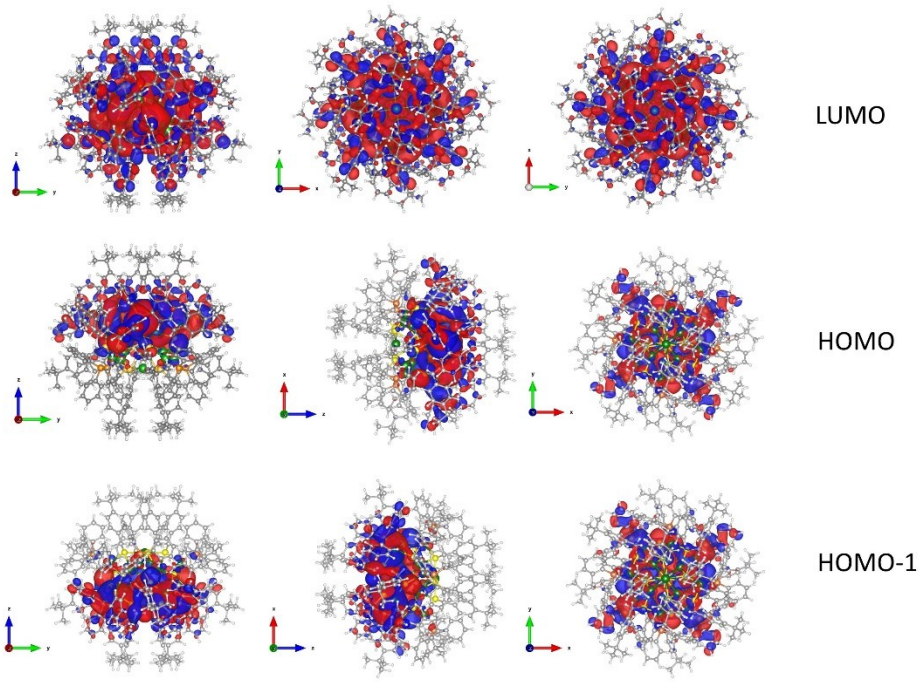

Figure S14 Ground states calculated LUMO, HOMO and HOMO-1 of Ag18S nanocluster.

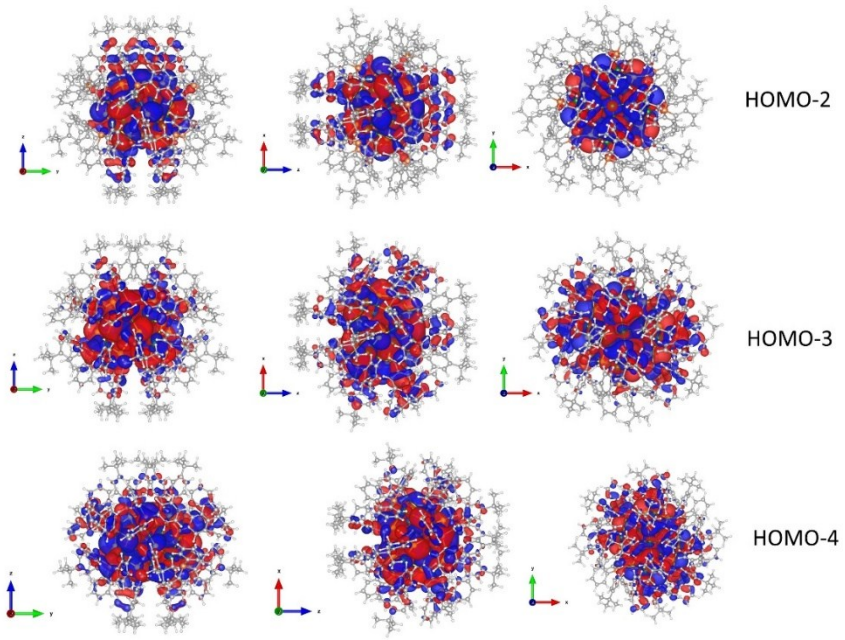

Figure S15 Visualization of the two distinct molecular states contributed to the visible absorption of $Ag_{18}S$ nanoclusters.

Supporting Tables

Table S1 Comparsion of the Ag and Pd molar ratio of the crystals obtained in one step crystalliztion and fractional crystalliztions.

		Ag (mg/L)	**Pd** (mg/L)	**Ag/Pd (mole ratio)**
1	**One step**	4.61	0.012	376.8
2	**Fraction 1**	20.51	0.006	3372.7
	Fraction 2	60.23	0.321	190.4
	Fraction 3	39.80	1.810	21.7

Table S2 Crystal data and structure refinement for $Ag_{18}S(p\text{-}TBBT)_{16}(PPh_3)_8$

Identification code	20190429_1
Empirical formula	C320H360Ag18P8S17
Formula weight	6940.50
Temperature/K	100.00(10)
Crystal system	tetragonal
Space group	P4/ncc
a/Å	26.69470(10)
b/Å	26.69470(10)
c/Å	50.0946(3)
α/°	90
β/°	90
γ/°	90
Volume/Å3	35697.8(3)
Z	4
ρcalcg/cm3	1.291
μ/mm-1	9.324
F(000)	14072.0
Crystal size/mm3	0.2 × 0.1 × 0.1
Radiation	CuKα (λ = 1.54184)
2Θ range for data collection/°	4.682 to 148.014
Index ranges	-31 ≤ h ≤ 32, -32 ≤ k ≤ 31, -51 ≤ l ≤ 61
Reflections collected	202082
Independent reflections	18035 [Rint = 0.0467, Rsigma = 0.0232]
Data/restraints/parameters	18035/14/858
Goodness-of-fit on F2	1.043
Final R indexes [I>=2σ (I)]	R1 = 0.0552, wR2 = 0.1533
Final R indexes [all data]	R1 = 0.0623, wR2 = 0.1599
Largest diff. peak/hole / e Å-3	1.33/-1.75

Table S3 Fractional atomic coordinates ($\times 10^4$) and equivalent isotropic displacement parameters ($Å^2 \times 10^3$) for $Ag_{18}S(p\text{-}TBBT)_{16}(PPh_3)_8$ nanoclusters. U_{eq} is defined as 1/3 of of the trace of the orthogonalised U_{IJ} tensor.

Atom	*x*	*y*	*z*	U(eq)
Ag_{1C}	1769.6(2)	1954.3(2)	1238.8(2)	52.93(11)
Ag_{1M}	2500	2500	328.3(2)	40.34(14)
Ag_{1P}	1115.6(2)	1499.5(2)	646.5(2)	67.90(14)
Ag_{2C}	2356.6(2)	1628.3(2)	763.1(2)	47.42(10)
Ag_{2M}	2500	2500	1668.9(2)	49.61(17)
Ag_{2P}	2215.1(2)	790.7(2)	1374.1(2)	74.44(15)
S_0	2500	2500	1010.6(5)	43.8(5)
S_{1T}	1881.2(5)	1761.0(5)	332.4(2)	48.6(3)
S_{2T}	1448.4(5)	1113.7(6)	1113.4(2)	59.3(3)
S_3	2725.2(5)	811.5(5)	902.1(2)	50.9(3)
S_{3T}	3453.9(6)	2596.6(5)	1664.7(2)	60.1(3)
P_1	2265.7(8)	11.1(7)	1629.4(3)	77.1(5)
P_5	589.5(5)	919.7(5)	392.5(2)	53.8(3)
C_{1P}	25(2)	682(2)	557.2(10)	59.1(13)
C_{1S}	3657(2)	3103(2)	1886.0(9)	55.6(12)
C_{2P}	-136(2)	191(2)	532.2(10)	58.4(13)
C_{3P}	-559(2)	25(3)	668.2(11)	66.6(15)
C_{4P}	-827(3)	351(3)	820.2(14)	80.6(19)
C_{5P}	-673(3)	847(3)	844.5(16)	90(2)
C_{6P}	-252(3)	1014(3)	713.8(13)	74.7(17)
C_{7P}	363(2)	1141.1(19)	71.9(9)	50.6(11)
C_{7S}	3443.5(17)	2577.7(16)	2294.1(8)	77.4(18)
C_{2S}	3731.8(17)	2949.1(15)	2174.9(6)	58.1(13)
C_{3S}	4092.7(19)	3201.4(17)	2323.0(9)	98(2)
C_{4S}	4165(2)	3082(2)	2590.3(9)	122(3)
C_{5S}	3877(3)	2711(2)	2709.5(6)	122(3)
C_{6S}	3516(2)	2458.5(18)	2561.4(8)	107(3)
C_{8P}	-73(2)	952(2)	-48.6(11)	59.4(13)
C_{9P}	-223(2)	1122(3)	-296.9(12)	69.3(16)
C_{10P}	51(2)	1495(3)	-424.2(13)	69.4(16)
C_{11P}	476(2)	1691(2)	-304.4(11)	59.3(13)
C_{12P}	635(2)	1514(2)	-58.9(10)	53.0(12)
C_{13P}	927(2)	350(2)	305.8(10)	52.6(11)
C_{14P}	1002(2)	191(2)	43.4(10)	57.1(12)
C_{15P}	1281(2)	-234(2)	-10.4(12)	63.7(14)
C_{16P}	1491(2)	-506(2)	195.0(14)	71.2(16)
C_{16S}	842(2)	1114(3)	1298.2(12)	67.9(15)
C_{17P}	1411(2)	-356(3)	458.8(13)	73.5(17)
C_{18P}	1137(2)	69(2)	512.2(11)	64.6(14)
C_{18S}	788.3(18)	449.1(16)	1653.6(6)	76.3(18)

C_{19S}	631.9(19)	-18.1(17)	1743.4(6)	86(2)
C_{20S}	376(2)	-338.5(14)	1572.4(8)	87(2)
C_{21S}	277(2)	-191.7(16)	1311.5(7)	90(2)
C_{22S}	433.0(18)	275.5(17)	1221.7(6)	80(2)
C_{17S}	688.8(18)	595.9(13)	1392.7(7)	68.2(16)
C_{19P}	2004(3)	-535(3)	1462.9(14)	89(2)
C_{20P}	2205(4)	-1009(4)	1493(2)	119(3)
C_{21P}	1978(5)	-1423(4)	1348(2)	133(4)
C_{22P}	1577(4)	-1311(5)	1189(2)	122(3)
C_{23P}	1383(4)	-861(4)	1159.2(17)	107(3)
C_{23S}	177(4)	-851(4)	1680.4(16)	105(3)
C_{24P}	1594(3)	-466(3)	1295.1(13)	90(2)
C_{24S}	-325(4)	-754(4)	1824(2)	134(4)
C_{25S}	90(4)	-1236(4)	1452.9(19)	128(4)
C_{26S}	561(5)	-1076(4)	1871(2)	149(5)
C_{27S}	2326(3)	398(3)	704.3(18)	112(4)
C_{28P}	3890(2)	-438(3)	1823.4(17)	153(4)
C_{29P}	3740(2)	-351(3)	1561.7(14)	127(3)
C_{30P}	3248(2)	-217(3)	1507.2(9)	108(3)
C_{25P}	2904.5(19)	-170(2)	1714.4(11)	89(2)
C_{26P}	3054(3)	-257(3)	1976.1(9)	146(4)
C_{27P}	3547(3)	-391(3)	2030.6(12)	182(6)
C_{31P}	1943.6(18)	20.7(17)	1951.2(7)	78.0(18)
C_{36P}	1871.0(19)	482.6(15)	2073.3(8)	76.8(18)
C_{35P}	1627(2)	509.9(18)	2318.0(8)	100(2)
C_{34P}	1456(2)	75(2)	2440.7(8)	115(3)
C_{33P}	1528(2)	-386.5(19)	2318.6(9)	114(3)
C_{32P}	1772(2)	-413.9(14)	2073.8(9)	99(2)
C_{36S}	2749(4)	-1860(3)	305(2)	108(5)
C_{37S}	3605(3)	-1601(3)	370.6(19)	100.0(17)
C_{46S}	2090.5(19)	1254.9(19)	107.9(9)	47.1(10)
C_{50S}	1639.1(13)	1405.1(11)	-714.0(4)	49.9(11)
C_{49S}	1723.1(13)	1833.8(9)	-563.1(5)	47.7(10)
C_{48S}	1870.1(12)	1792.2(9)	-297.8(5)	44.5(10)
C_{47S}	1933.2(12)	1321.9(11)	-183.5(4)	43.2(10)
C_{52S}	1849.2(13)	893.2(8)	-334.5(5)	49.5(11)
C_{51S}	1702.1(14)	934.8(9)	-599.8(5)	54.5(12)
C_{53S}	1457(2)	1469(2)	-1009.3(9)	56.9(12)
C_{54S}	1335(3)	967(3)	-1140.4(11)	82(2)
C_{55S}	1871(2)	1710(3)	-1174.6(11)	66.2(15)
C_{56S}	984(2)	1807(3)	-1017.4(10)	68.0(16)
C_{8S}	4208(5)	2609(5)	2989(2)	77.9(15)
C_{9S}	4782(5)	2454(6)	2977(2)	77.9(15)
C_{10S}	4179(7)	3093(6)	3151(2)	77.9(15)
C_{15S}	3968(7)	2174(6)	3109(3)	77.9(15)

C_{33S}	2561(3)	-543(3)	746.8(12)	54(3)
C_{32S}	2744(3)	-969(2)	620.2(14)	57(3)
C_{31S}	2897(3)	-944(2)	355.3(14)	50(3)
C_{30S}	2868(3)	-494(2)	217.1(11)	47(2)
C_{29S}	2686(3)	-68(2)	343.6(13)	47(3)
C_{28S}	2532(4)	-92(2)	608.5(14)	44(4)
C_{34S}	3085(6)	-1423(6)	213(4)	100.0(17)
C_{35S}	3153(7)	-1348(7)	-92(4)	100.0(17)
C_{11S}	4039(6)	2878(5)	3194(2)	77.9(15)
C_{12S}	3740(4)	2519(4)	3016.8(19)	66(3)
C_{13S}	3985(6)	1968(5)	3024(2)	77.9(15)
C_{14S}	3229(4)	2470(5)	3126(2)	77.9(15)
C_{38S}	3147(6)	-1909(6)	839(3)	100.0(17)
C_{39S}	3127(6)	-1640(5)	554(3)	100.0(17)
C_{40S}	2989(5)	-1079(4)	589(2)	65(3)
C_{41S}	2983(6)	-757(5)	368(3)	69(4)
C_{42S}	2815(5)	-267(5)	392(2)	64(4)
C_{43S}	2634(8)	-71(5)	634(3)	70(5)
C_{44S}	2648(5)	-399(4)	851(2)	57(3)
C_{45S}	2813(4)	-889(4)	833(2)	59(3)
H_{1SA}	1030.95	1760.16	1818.45	67
H_{1SB}	1590.67	1632.29	1881.43	67
H_{2P}	42.49	-32.22	424.87	71
H_{3P}	-656.34	-309.26	656.12	82
H_{4P}	-1114.87	241.72	908.75	99
H_{5P}	-860.66	1068.56	947.52	110
H_{6P}	-149.18	1347.24	729.02	92
H_{7S}	1762.81	2600.51	2249.73	83
H_{3S}	710.6	1530.85	2185.32	100
H_{4S}	447.7	1697.78	2617.69	126
H_{6S}	1499.9	2767.45	2682.1	74
H_{8P}	-262.08	710.67	39.12	72
H_{9P}	-502.8	991.02	-378.25	84
H_{10P}	-54.77	1611.5	-589.72	83
H_{11P}	652.22	1944.39	-390.13	71
H_{12P}	925.21	1639.87	19.44	65
H_{14P}	863.2	371.8	-95.79	68
H_{15P}	1329.35	-332.17	-186.77	77
H_{16P}	1677.86	-789.33	158.31	86
H_{16A}	868.05	1334.87	1449.35	84
H_{16B}	582.24	1244.22	1180.33	84
H_{17P}	1545.1	-536.36	599.66	89
H_{18P}	1092.99	169.81	688.83	77
H_{18S}	963.75	661.36	1766.69	97
H_{19S}	697.9	-115.88	1917.92	108

H_{21S}	97.05	-403.27	1198.56	112
H_{22S}	362.9	373.96	1047.33	102
H_{20P}	2484.94	-1071.37	1606.92	147
H_{21P}	2106.94	-1741.28	1367.22	174
H_{22P}	1423.64	-1587.47	1097.78	165
H_{23P}	1114.59	-813.46	1047.17	143
H_{24P}	1453.55	-142.51	1273.91	114
H_{24A}	-261.03	-541.03	1972.16	223
H_{24B}	-449.16	-1073.43	1886.18	223
H_{24C}	-551	-609.07	1702.45	223
H_{25A}	-182.63	-1120.68	1340.09	197
H_{25B}	1.12	-1555.19	1526.45	197
H_{25C}	385.7	-1268.18	1346.06	197
H_{26A}	866.91	-1141.3	1779.22	246
H_{26B}	430.32	-1387.6	1942.26	246
H_{26C}	617.95	-848.52	2015.85	246
H_{27A}	2028.2	330.78	801.9	122
H_{27B}	2233.33	579.35	542.28	122
H_{27C}	2038.35	295.8	802.28	122
H_{27D}	2220.15	568.68	541.35	122
H_{28P}	4223.49	-515.46	1859.09	163
H_{29P}	3968.43	-383.76	1421.96	163
H_{30P}	3144.51	-164.98	1331.86	163
H_{26P}	2830.68	-209.59	2116.02	163
H_{27P}	3654.6	-428.37	2206.13	163
H_{36P}	1989.14	772.18	1992.58	97
H_{35P}	1581.86	817.86	2400.97	128
H_{34P}	1292.83	92.91	2604.74	155
H_{33P}	1411.09	-677.72	2400.12	158
H_{32P}	1818.38	-723.41	1991.73	132
H_{36A}	2887.13	-2169.28	246.87	178
H_{36B}	2413.78	-1823.12	230.13	178
H_{36C}	2719.7	-1857.56	496.62	178
H_{36D}	2474.27	-2051.17	381.38	178
H_{36E}	2933.42	-2066.43	186.44	178
H_{36F}	2606.65	-1580.2	208.26	178
H_{37A}	3524.22	-1715.18	552.9	178
H_{37B}	3836.75	-1323.71	389.57	178
H_{37C}	3767.01	-1869.4	280.07	178
H_{37D}	3596.71	-1851.71	239.28	178
H_{37E}	3902.09	-1654.35	485.03	178
H_{37F}	3625.3	-1275.22	296.98	178
H_{46A}	2454.47	1234.33	115.3	57
H_{46B}	1959.42	938.76	172.47	57
H_{49S}	1680.17	2148.8	-639.38	58

H_{48S}	1926.98	2078.49	-196.91	53
H_{52S}	1890.9	578.13	-258.9	60
H_{51S}	1644.08	648.43	-701.37	67
H_{54A}	1626.68	758.17	-1139.85	125
H_{54B}	1226.32	1022.9	-1320.17	125
H_{54C}	1070.81	803.88	-1041.88	125
H_{55A}	1969.23	2022.17	-1095.22	101
H_{55B}	1754.32	1767.32	-1352.85	101
H_{55C}	2157.81	1489.42	-1180.31	101
H_{56A}	716.53	1649.65	-922.37	104
H_{56B}	889.38	1864.36	-1198.7	104
H_{56C}	1061.5	2124.45	-933.53	104
H_{9SA}	174.12	2884.28	2926.44	136
H_{9SB}	62.24	2495.65	3153.35	136
H_{9SC}	40.51	2329.05	2853.49	136
H_{10A}	529.22	1717.49	3115.47	175
H_{10B}	814.48	2008.51	3340.8	175
H_{10C}	1115.77	1745.38	3111.68	175
H_{15A}	1423.06	2799.37	3076.28	200
H_{15B}	998.04	2883.32	3287.55	200
H_{15C}	965.26	3143.9	3007.64	200
H_{33S}	2465.45	-571.24	925.28	67
H_{32S}	2765.35	-1277.46	707.77	69
H_{30S}	2964.05	-468.43	39.65	59
H_{29S}	2664.15	237.79	257.17	57
H_{35A}	3203.66	-1667.84	-176.46	178
H_{35B}	3434.11	-1135.89	-126.45	178
H_{35C}	2855.38	-1195.19	-169.19	178
H_{11A}	625.06	2109.47	3135.15	120
H_{11B}	988.95	2221.87	3373.36	120
H_{11C}	1107.86	1783.57	3174.95	120
H_{13A}	1182.61	3249.73	2941.26	147
H_{13B}	907.62	3086.49	3203.74	147
H_{13C}	668.08	2968.3	2925.04	147
H_{14A}	1968.85	2228.16	3096.16	101
H_{14B}	1760.05	2587.35	3317.33	101
H_{14C}	1947.24	2807.05	3044.79	101
H_{38A}	2833.86	-1837.65	940.76	178
H_{38B}	3420.83	-1819.41	942.54	178
H_{38C}	3142.67	-2278.67	815.78	178
H_{41S}	3099.61	-872.13	202.62	91
H_{42S}	2833.89	-76.35	236.02	74
H_{44S}	2531.29	-266.92	1009.99	68
H_{45S}	2792.22	-1094.16	984.35	68
H_{6T}	1841.72	2775.33	2610.99	68

H_{7T}	1799.94	2582.89	2149.7	78
H_{3T}	756.29	1582.65	2298.08	88
H_{4T}	720.88	1768.75	2726.29	93

Table S4 Atomic Occupancy for $Ag_{18}S(p\text{-}TBBT)_{16}(PPh_3)_8$ nanocluster.

Atom	***Occupancy***	**Atom**	***Occupancy***	**Atom**	***Occupancy***
C_{7S}	0.515	H_{7S}	0.515	C_{3S}	0.515
H_{3S}	0.515	C_{4S}	0.515	H_{4S}	0.515
C_{5S}	0.515	C_{6S}	0.515	H_{6S}	0.515
H_{27A}	0.518(9)	H_{27B}	0.518(9)	H_{27C}	0.482(9)
H_{27D}	0.482(9)	H_{36A}	0.518(9)	H_{36B}	0.518(9)
H_{36C}	0.518(9)	H_{36D}	0.482(9)	H_{36E}	0.482(9)
H_{36F}	0.482(9)	H_{37A}	0.518(9)	H_{37B}	0.518(9)
H_{37C}	0.518(9)	H_{37D}	0.482(9)	H_{37E}	0.482(9)
H_{37F}	0.482(9)	C_{8S}	0.515	C_{9S}	0.515
H_{9SA}	0.515	H_{9SB}	0.515	H_{9SC}	0.515
C_{10S}	0.515	H_{10A}	0.515	H_{10B}	0.515
H_{10C}	0.515	C_{15S}	0.515	H_{15A}	0.515
H_{15B}	0.515	H_{15C}	0.515	C_{33S}	0.518(9)
H_{33S}	0.518(9)	C_{32S}	0.518(9)	H_{32S}	0.518(9)
C_{31S}	0.518(9)	C_{30S}	0.518(9)	H_{30S}	0.518(9)
C_{29S}	0.518(9)	H_{29S}	0.518(9)	C_{28S}	0.518(9)
C_{34S}	0.518(9)	C_{35S}	0.4579	H_{35A}	0.4579
H_{35B}	0.4579	H_{35C}	0.4579	C_{11S}	0.485
H_{11A}	0.485	H_{11B}	0.485	H_{11C}	0.485
C_{12S}	0.485	C_{13S}	0.485	H_{13A}	0.485
H_{13B}	0.485	H_{13C}	0.485	C_{14S}	0.485
H_{14A}	0.485	H_{14B}	0.485	H_{14C}	0.485
C_{38S}	0.5421	H_{38A}	0.5421	H_{38B}	0.5421
H_{38C}	0.5421	C_{39S}	0.482(9)	C_{40S}	0.482(9)
C_{41S}	0.482(9)	H_{41S}	0.482(9)	C_{42S}	0.482(9)
H_{42S}	0.482(9)	C_{43S}	0.482(9)	C_{44S}	0.482(9)
H_{44S}	0.482(9)	C_{45S}	0.482(9)	H_{45S}	0.482(9)
C_{5T}	0.485	C_{6T}	0.485	H_{6T}	0.485
C_{7T}	0.485	H_{7T}	0.485	C_{3T}	0.485
H_{3T}	0.485	C_{4T}	0.485	H_{4T}	0.485

Table S5. Comparisons of the Ag-S bonds in square-like Ag_5S_4 units in $Ag_{18}S$ nanocluster and the reported nanocluster structures.

Cluster structure	Bond length of S-Ag (Å)		Refs
	Minimum	Maximum	
$Ag_{18}S$	2.483	2.730	This Work
Ag_{14}	2.528	2.657	[20]
$Ag_{14}S$	2.416	2.717	[21]
$Ag_{62}S_{13}^{4+}$	2.533	2.618	[22]
$Ag_{62}S_{12}^{2+}$	2.537	2.626	[23]

Table S6. Comparisons between the bond lengths of sulfide-metal in $Ag_{18}S$ nanocluster and the reported nanocluster structures.

Cluster structure	Coordinating type	Bond length of sulfide-metal (Å)		Refs
		Minimum	Maximum	
$Ag_{18}S$	**μ_8-**	2.664	2.689	The work
$Ag_{344}S_{124}$	**μ_7-**	2.585	2.937	[24]
$Ag_{62}S_{13}^{4+}/Ag_{62}S_{12}^{2+}$	**μ_6-**	2.398	2.814	[22-23]
$Ag_{344}S_{124}$	**μ_5-**	2.346	2.953	[24]
$Ag_{46}S_7$	**μ_4-**	2.136	2.385	[25]
$Ag_{115}S_{34}$	**μ_3-**		ave. 2.53	[26]
$Ag_{115}S_{34}$	**μ_2-**	2.340	2.580	[26]

Table S7 Net atomic charge populations of $Ag_{18}S$ (Top), Ag_{33} (Middle) and Ag_{23} (Bottom) nanoclusters[a] derived from the density derived electrostatic and chemical (DDEC) method.

Core		**Shell**				**R group**	
S_O	Ag_C	Ag_M	Ag_P	S_T	P	C	H
-0.53077	0.191(2)	0.18455(3)	0.063(1)	-0.271(8)	0.2882(6)	-0.44~0.26	0.11(2)
For $Ag_{18}S$ nanocluster Average S: ~-0.28 (~-0.27 except for S_o); Average Ag: ~0.13							

Core		**Shell**						**R group**	
Ag_C	Ag_I	Ag_S	Ag_T	Ag_B	S_1	S_2	P	C	H
-0.09650	0.014(8)	0.12(3)	0.060(3)	0.09(2)	-0.198(7)	-0.246(7)	0.2838(7)	-0.20~0.12	0.09(2)
For Ag_{33} nanocluster Average S: ~-0.22; Average Ag: ~ 0.07									

Kernel framework					**R group**		
Ag_F	Ag_C	Ag_R	μ_5-S	μ_4-S	P	C	H
0.07-0.16	-0.1479	0.04-0.11	-0.212(1)	-0.24(3)	0.272(6)	-0.20-0.13	0.07-0.11
For Ag_{23} nanocluster Average S: ~-0.24; Average Ag: ~0.08							

[a]. The core, shell categories and the atomic labels of $Ag_{18}S$ and Ag_{33} nanocluster are identical to the main article and the previous Ag_{33} report[1], respectively. The atomic labels of Ag_{23} nanocluster are according to the reported structure[2]. The Ag atoms in the rhombic bipyramids except for the central one are labeled as Ag_R; the

central Ag and the rest Ag atoms are labeled as Ag_C and Ag_F, respectively. The S atoms are labeled according to their coordinating numbers (including C atoms). The numbers in parentheses denote the errors, ie. -0.271(8) equals to -0.271±0.008.

Reference

1. Tian, F.; Chen, R., *J. Am. Chem. Soc.* **2019,** *141* (17), 7107-7114.
2. Liu, C.; Li, T.; Abroshan, H.; Li, Z.; Zhang, C.; Kim, H. J.; Li, G.; Jin, R., *Nat. Commun.* **2018,** *9* (1), 744.
3. Hutter, J.; Iannuzzi, M.; Schiffmann, F.; VandeVondele, J., *Wires. Comput. Mol. Sci.* **2014,** *4* (1), 15-25.
4. VandeVondele, J.; Krack, M.; Mohamed, F.; Parrinello, M.; Chassaing, T.; Hutter, J., *Comput. Phys. Commun.* **2005,** *167* (2), 103-128.
5. VandeVondele, J.; Hutter, J., *J. Chem. Phys.* **2007,** *127* (11), 114105.
6. Goedecker, S.; Teter, M.; Hutter, J., *Physical Review B* **1996,** *54* (3), 1703-1710.
7. Hartwigsen, C.; Goedecker, S.; Hutter, J., *Physical Review B* **1998,** *58* (7), 3641-3662.
8. Krack, M., *Theor. Chem. Acc.* **2005,** *114* (1), 145-152.
9. Perdew, J. P.; Burke, K.; Ernzerhof, M., *Phys. Rev. Lett.* **1996,** *77* (18), 3865-3868.
10. Manz, T. A.; Sholl, D. S., *J. Chem. Theory Comput.* **2010,** *6* (8), 2455-2468.
11. Limas, N. G.; Manz, T. A., *RSC Adv.* **2016,** *6* (51), 45727-45747.
12. Manz, T. A.; Limas, N. G., *RSC Adv.* **2016,** *6* (53), 47771-47801.
13. Lu, T.; Chen, F., *J. Comput. Chem.* **2011,** *33* (5), 580-592.
14. Momma, K.; Izumi, F., *J. Appl. Crystallogr.* **2011,** *44* (6), 1272-1276.
15. M. J. Frisch, G. W. T., H. B. Schlegel, G. E. Scuseria, ; M. A. Robb, J. R. C., G. Scalmani, V. Barone, ; G. A. Petersson, H. N., X. Li, M. Caricato, A. V. Marenich, ; J. Bloino, B. G. J., R. Gomperts, B. Mennucci, H. P. Hratchian, ; J. V. Ortiz, A. F. I., J. L. Sonnenberg, D. Williams-Young, ; F. Ding, F. L., F. Egidi, J. Goings, B. Peng, A. Petrone, ; T. Henderson, D. R., V. G. Zakrzewski, J. Gao, N. Rega, ; G. Zheng, W. L., M. Hada, M. Ehara, K. Toyota, R. Fukuda, ; J. Hasegawa, M. I., T. Nakajima, Y. Honda, O. Kitao, H. Nakai, ; T. Vreven, K. T., J. A. Montgomery, Jr., J. E. Peralta, ; F. Ogliaro, M. J. B., J. J. Heyd, E. N. Brothers, K. N. Kudin, ; V. N. Staroverov, T. A. K., R. Kobayashi, J. Normand, ; K. Raghavachari, A. P. R., J. C. Burant, S. S. Iyengar, ; J. Tomasi, M. C., J. M. Millam, M. Klene, C. Adamo, R. Cammi, ; J. W. Ochterski, R. L. M., K. Morokuma, O. Farkas, ; J. B. Foresman, a. D. J. F., *Gaussian Inc.: Wallingford CT*.
16. Rigaku Oxford Diffraction, x., *Rigaku Corporation, Oxford, UK*.
17. Dolomanov, O. V.; Bourhis, L. J.; Gildea, R. J.; Howard, J. A. K.; Puschmann, H., *J. Appl. Crystallogr.* **2009,** *42* (2), 339-341.
18. Sheldrick, G. M., *Acta Cryst. A* **2008,** *64* (Pt 1), 112-22.
19. Sheldrick, G. M., *Acta Cryst. C* **2015,** *71* (Pt 1), 3-8.
20. Yang, H.; Lei, J.; Wu, B.; Wang, Y.; Zhou, M.; Xia, A.; Zheng, L.; Zheng, N., *Chem. Commun.* **2013,** *49* (3), 300-302.
21. Jin, X.; Tang, K.; Liu, W.; Zeng, H.; Zhao, H.; Ouyang, Y.; Tang, Y., *Polyhedron* **1996,** *15* (7), 1207-1211.
22. Li, G.; Lei, Z.; Wang, Q. M., *J. Am. Chem. Soc.* **2010,** *132* (50), 17678-9.
23. Jin, S.; Wang, S.; Song, Y.; Zhou, M.; Zhong, J.; Zhang, J.; Xia, A.; Pei, Y.; Chen, M.; Li, P.; Zhu, M., *J. Am. Chem. Soc.* **2014,** *136* (44), 15559-65.
24. Fenske, D.; Anson, C. E.; Eichhofer, A.; Fuhr, O.; Ingendoh, A.; Persau, C.; Richert, C., *Angew. Chem. Int. Ed.* **2005,** *44* (33), 5242-6.
25. Liu, X.; Chen, J.; Yuan, J.; Li, Y.; Li, J.; Zhou, S.; Yao, C.; Liao, L.; Zhuang, S.; Zhao, Y.; Deng, H.; Yang, J.; Wu, Z., *Angew. Chem. Int. Ed.* **2018,** *57* (35), 11273-11277.
26. Bestgen, S.; Fuhr, O.; Breitung, B.; Kiran Chakravadhanula, V. S.; Guthausen, G.; Hennrich, F.; Yu, W.; Kappes, M. M.; Roesky, P. W.; Fenske, D., *Chem. Sci.* **2017,** *8* (3), 2235-2240.